applied sciences

MDPI

Article

Buckling Enhancement Analysis of Auxetic Laminated Rectangular Plate under Uniaxial Compression

Kai Wang [1], Feng Wan [1], Ling Luo [1,*], Pengyu Cao [1], Lei Han [1] and Peng Jin [2]

[1] Aerospace Institute of Advanced Materials and Processing Technology, Beijing 100074, China; wangktju@163.com (K.W.)
[2] School of Aerospace Engineering, Huazhong University of Science & Technology, Wuhan 430074, China
* Correspondence: luoling_buaa@yeah.net

Abstract: The buckling enhancement of the negative Poisson's ratio (NPR) effect on a laminated plate under uniaxial compression with an in-plane translational restraint is investigated in this paper. According to the buckling equation of an orthotropic plate under biaxial compression, the critical buckling load of an NPR-laminated composite under uniaxial compression can be increased due to the induced tension force on the unloaded direction. Instead of layer angles and stacking sequence, the NPR envelope and buckling load enhancement are studied using lamination parameters in this paper. The Poisson's ratio contours are given in the feasible region of membrane lamination parameters. The results show that the negative Poisson's ratios are more sensitive to V_3^A, which represents the unbalance degree of the laminate. Furthermore, the buckling loads for various Poisson's ratio layups are investigated, and it is concluded that the buckling load increases with a decrease in Poisson's ratio for the laminated rectangular plate considering in-plane translational restraint. Finally, the inverse problem of deciding the laminate configuration to target the lamination parameters is solved using the particle swarm optimization (PSO) algorithm.

Keywords: buckling; laminated structure; negative Poisson's ratio (NPR); lamination parameters; PSO

Citation: Wang, K.; Wan, F.; Luo, L.; Cao, P.; Han, L.; Jin, P. Buckling Enhancement Analysis of Auxetic Laminated Rectangular Plate under Uniaxial Compression. *Appl. Sci.* **2023**, *13*, 6244. https://doi.org/10.3390/app13106244

Academic Editor: Francesco Clementi

Received: 31 March 2023
Revised: 15 May 2023
Accepted: 16 May 2023
Published: 19 May 2023

1. Introduction

Auxetics which possess negative Poisson's ratios show a transverse expansion or contraction effect under uniaxial tension or compression load, respectively. The counter-intuitive properties of tension–expansion deformation lead to enhanced mechanical and other physical performances, such as large plane strain fracture toughness, high shear modulus, low fatigue crack propagation rate, superior specific strength, excellent shock and sound absorption, etc. [1–5] Since Lakes [6] manufactured a novel foam structure with a negative Poisson's ratio (NPR) of −0.7, a variety of cellular structures with auxetic features have been proposed from nano-scale to macro-scale levels [7]. However, the low mechanical performance of auxetic cellular structures largely restricts their applications, especially in load-bearing fields [8].

By changing the orientation or stacking sequence of laminate layers, laminated structures with auxetic properties can be obtained with excellent mechanical performance. The Poisson's ratio cannot take a negative value according to experimental investigations, however, for laminated composites, the inter-laminar stresses cause overall auxetic behavior which can be controlled by special layup [9]. Herakovich [10] reported an early work on composite laminates with out-of-plane negative Poisson's ratios and concluded that the Poisson's ratios can be positive or negative, mainly depending on fiber orientation. The out-of-plane NPR can affect the vibration [11], dynamic responses [12] and low velocity impact [13] responses of laminated structures. For in-plane NPR, Miki [14] studied the unique behavior of the Poisson's ratio of laminated composites and observed a minimum value of Poisson's ratio of −0.369 for unbalanced bi-directional laminates. Shokrieh [9] used

GA to obtain the minimum negative Poisson's ratio of −0.3536 for a laminated composite plate with the configuration of (15/60/15).

Buckling is a common failure mode for an aerospace structure under compression. Many researchers have studied the buckling of rectangular composite plates [15,16], and the buckling behavior of auxetic materials has also received significant attention. Zhang [17] indicates that the buckling performance of a rectangular plate under uniaxial compression can be significantly improved by replacing the traditional material, that has a positive Poisson's ratio, with an auxetic material. Shen [18,19] reported that the post-buckling behaviors of pressure-loaded graphene-reinforced metal-matrix-composite laminated cylindrical shells are affected substantially by the in-plane NPR. Kennedy studied the analysis and design of composite structural components such as fuselage and wings, and proposed optimization methods [20].

The aim of this study is to investigate the buckling enhancement of a laminated rectangular plate under uniaxial compression through an auxetic composite layup design. As a brief representation of laminate stiffness, lamination parameters are employed to obtain the NPR envelope and buckling load with negative Poisson's ratio. The structure of this paper is as follows: firstly, the Poisson's ratio of laminated structures and feasible region of lamination parameters are described briefly. Next, a mechanism analysis of the enhanced buckling for the laminated orthotropic auxetic plate is provided in Section 3. Section 4 introduces the results and discussion for various lamination parameters and Poisson's ratios. Finally, Section 5 gives the conclusion.

2. Classical Laminate Theory and Lamination Parameters

2.1. Lamination Parameters and Feasible Region

The laminate constitutive equation of strain–load intensity relationships according to classical laminate theory [21] is as follows:

$$\begin{Bmatrix} N \\ M \end{Bmatrix} = \begin{bmatrix} A_{ij} B_{ij} \\ B_{ij} D_{ij} \end{bmatrix} \begin{Bmatrix} \varepsilon \\ k \end{Bmatrix} \tag{1}$$

in which N and M denote the force and moment resultants, respectively. ε and k denote normal and shear strains. A_{ij}, B_{ij}, and D_{ij} are the elements of the membrane stiffness matrix, the membrane-bending coupling matrix, and the bending matrix of the laminate, respectively. A_{ij}, B_{ij}, and D_{ij} can be expressed in terms of 12 lamination parameters and material stiffness invariants U.

$$\begin{Bmatrix} A_{11} \\ A_{22} \\ A_{12} \\ A_{66} \\ A_{16} \\ A_{26} \end{Bmatrix} = h \begin{bmatrix} U_1 & V_1^A & V_2^A \\ U_1 & -V_1^A & V_2^A \\ U_4 & 0 & -V_2^A \\ U_5 & 0 & -V_2^A \\ 0 & \frac{V_3^A}{2} & V_4^A \\ 0 & \frac{V_3^A}{2} & V_4^A \end{bmatrix} \begin{Bmatrix} 1 \\ \\ U_2 \\ \\ U_3 \end{Bmatrix} \tag{2}$$

$$\begin{Bmatrix} B_{11} \\ B_{22} \\ B_{12} \\ B_{66} \\ B_{16} \\ B_{26} \end{Bmatrix} = \frac{h^2}{4} \begin{bmatrix} V_1^B & V_2^B \\ -V_1^B & V_2^B \\ 0 & -V_2^B \\ 0 & -V_2^B \\ \frac{V_3^B}{2} & V_4^B \\ \frac{V_3^B}{2} & -V_4^B \end{bmatrix} \begin{Bmatrix} U_2 \\ \\ U_3 \end{Bmatrix} \tag{3}$$

$$\begin{Bmatrix} D_{11} \\ D_{22} \\ D_{12} \\ D_{66} \\ D_{16} \\ D_{26} \end{Bmatrix} = \frac{h^3}{12} \begin{bmatrix} U_1 & V_1^D & V_2^D \\ U_1 & -V_1^D & V_2^D \\ U_4 & 0 & -V_2^D \\ U_5 & 0 & -V_2^D \\ 0 & \frac{V_3^D}{2} & V_4^D \\ 0 & \frac{V_3^D}{2} & -V_4^D \end{bmatrix} \begin{Bmatrix} 1 \\ \\ U_2 \\ \\ U_3 \end{Bmatrix} \tag{4}$$

The material stiffness invariants U are calculated as follows:

$$\begin{Bmatrix} U_1 \\ U_2 \\ U_3 \\ U_4 \\ U_5 \end{Bmatrix} = \frac{1}{8} \begin{bmatrix} 3 & 2 & 3 & 4 \\ 4 & 0 & -4 & 0 \\ 1 & -2 & 1 & -4 \\ 1 & 6 & 1 & -4 \\ 1 & -2 & 1 & 4 \end{bmatrix} \begin{Bmatrix} Q_{11} \\ Q_{12} \\ Q_{22} \\ Q_{66} \end{Bmatrix} \tag{5}$$

where $Q_{11} = \frac{E_{11}}{1-\nu_{12}\nu_{21}}$, $Q_{22} = \frac{E_{22}}{1-\nu_{12}\nu_{21}}$, $Q_{21} = Q_{12} = \frac{\nu_{12}E_2}{1-\nu_{12}\nu_{21}}$, $Q_{66} = G_{12}$, and $\nu_{21} = \nu_{12}\frac{E_{22}}{E_{11}}$.

The membrane, coupling, and bending lamination parameters are given, respectively, by the following integrals:

$$V^{\mathrm{A}}_{[1\ 2\ 3\ 4]} = \frac{1}{h}\int_{-h/2}^{h/2} [\cos 2\theta \quad \cos 4\theta \quad \sin 2\theta \quad \sin 4\theta] dz \tag{6}$$

$$V^{\mathrm{B}}_{[1\ 2\ 3\ 4]} = \frac{4}{h^2}\int_{-h/2}^{h/2} [\cos 2\theta \quad \cos 4\theta \quad \sin 2\theta \quad \sin 4\theta] z dz \tag{7}$$

$$V^{\mathrm{D}}_{[1\ 2\ 3\ 4]} = \frac{12}{h^3}\int_{-h/2}^{h/2} [\cos 2\theta \quad \cos 4\theta \quad \sin 2\theta \quad \sin 4\theta] z^2 dz \tag{8}$$

Lamination parameters cannot be arbitrarily prescribed since the trigonometric functions entering their definition are related. For a symmetric laminate, the number of independent lamination parameters can be reduced to eight. The feasible domain for membrane and bending lamination parameters for symmetric laminate is known to be convex and defined by [21–23].

$$2(V_1^X)^2 - V_2^X - 1 \le 0, \quad X = A, D \tag{9a}$$

$$2(V_1^X)^2 - V_3^X - 1 \le 0, \quad X = A, D \tag{9b}$$

$$2(1+V_2^X)^2 V_3^X - 4V_1^X V_3^X V_4^X + (V_4^X)^2 - (V_2^X - 2(V_1^X)^2 + 1)(1 - V_2^X) \le 0, \quad X = A, D \tag{9c}$$

$$4(V_i^D - 1)(V_i^A - 1) \le (V_i^A - 1)^4, \quad i = 1, 2, 3 \tag{9d}$$

$$4(V_i^D + 1)(V_i^A + 1) \le (V_i^A + 1)^4, \quad i = 1, 2, 3 \tag{9e}$$

2.2. Poisson's Ratio of the Laminate [24]

According to Equation (1):

$$\begin{Bmatrix} N_x \\ N_y \\ N_{xy} \end{Bmatrix} = [A] \begin{Bmatrix} \varepsilon_x \\ \varepsilon_y \\ \gamma_{xy} \end{Bmatrix} \tag{10}$$

in which N_x, N_y, and N_{xy} denote the inner forces in the longitudinal (x) direction, transverse (y) direction, and in-plane shear force resultants per unit length (load intensities), respectively. We can express the strains as functions of the applied load intensities by:

$$\begin{Bmatrix} \varepsilon_x \\ \varepsilon_y \\ \gamma_{xy} \end{Bmatrix} = \left[A^{-1}\right] \begin{Bmatrix} N_x \\ N_y \\ N_{xy} \end{Bmatrix} \tag{11}$$

where $[A^{-1}]$ is the inverse of the matrix $[A]$. For a symmetric laminate, it may be shown that the in-plane load intensities do not produce out-of-plane curvature deformations. The average direct stresses across the thickness of the laminate as:

$$\overline{\sigma}_x = \frac{N_x}{t},\ \overline{\sigma}_y = \frac{N_y}{t},\ \overline{\tau}_{xy} = \frac{N_{xy}}{t} \tag{12}$$

Equation (10) then becomes:

$$\begin{Bmatrix} \varepsilon_x \\ \varepsilon_y \\ \gamma_{xy} \end{Bmatrix} = t\left[A^{-1}\right] \begin{Bmatrix} \overline{\sigma}_x \\ \overline{\sigma}_y \\ \overline{\tau}_{xy} \end{Bmatrix} \tag{13}$$

Let the terms in $[A^{-1}]$ be as follows:

$$\left[A^{-1}\right] = \begin{bmatrix} a_{11} & a_{12} & a_{16} \\ a_{12} & a_{22} & a_{26} \\ a_{16} & a_{26} & a_{66} \end{bmatrix} \tag{14}$$

Suppose, now, that a symmetric laminate is subjected to a single load intensity, N_x. Then:

$$\overline{\sigma}_x = \frac{N_x}{t},\ \overline{\sigma}_y = 0,\ \overline{\tau}_{xy} = 0 \tag{15}$$

From Equations (13) and (14), Young's modulus for the laminate in the x direction:

$$E_x = \overline{\sigma}_x/\varepsilon_x = \frac{1}{ta_{11}} \tag{16}$$

$$\varepsilon_y = ta_{12}\overline{\sigma}_x = ta_{12}\varepsilon_x/ta_{11} = (a_{12}/a_{11})\varepsilon_x \tag{17}$$

Equation (17) gives the strain in the y direction due to a load in the x direction, that is the Poisson's effect. Then, Poisson's ratio in the xy plane of the laminate is given by:

$$v_{xy} = \frac{-\varepsilon_y}{\varepsilon_x} = \frac{-a_{12}}{a_{11}} = \frac{A_{16}A_{26} - A_{12}A_{66}}{A_{22}A_{66} - A_{26}A_{26}} \tag{18}$$

The above arguments may be applied to a symmetric laminate subjected to a single load intensity, N_y. Then, Young's modulus for the laminate in the y direction and Poisson's ratio in the xy plane are:

$$E_y = \overline{\sigma}_y/\varepsilon_y = \frac{1}{ta_{22}} \tag{19}$$

$$v_{yx} = \frac{-a_{12}}{a_{22}} = \frac{A_{16}A_{26} - A_{12}A_{66}}{A_{11}A_{66} - A_{16}A_{16}} \tag{20}$$

According to Equations (2), (18) and (20), Poisson's ratios of v_{xy} and v_{yx} are not dependent on the stacking sequences of laminated composites and just functions of membrane stiffness matrix elements or membrane lamination parameters. Poisson's ratio envelope can be studied by using membrane lamination parameters as design variables.

3. Buckling of Laminated Plate with In-Plane Translational Restraint

The derivation of the buckling equation of a rectangular orthotropic plate under a biaxial load follows the approach described by Whitney [25]. The Rectangular composite panel under biaxial loading is shown in Figure 1. It is convenient to let $k = N_y/N_x$ and to let the buckling load N_x be denoted by $-N_{cr}$ (minus sign to indicate compression):

$$N_{cr}(m,n) = \frac{D_{11}(m\pi/a)^4 + 2(D_{12} + 2D_{66})(m\pi/a)^2(n\pi/b)^2 + D_{22}(n\pi/b)^4}{(m\pi/a)^2 + k(n\pi/b)^2} \tag{21}$$

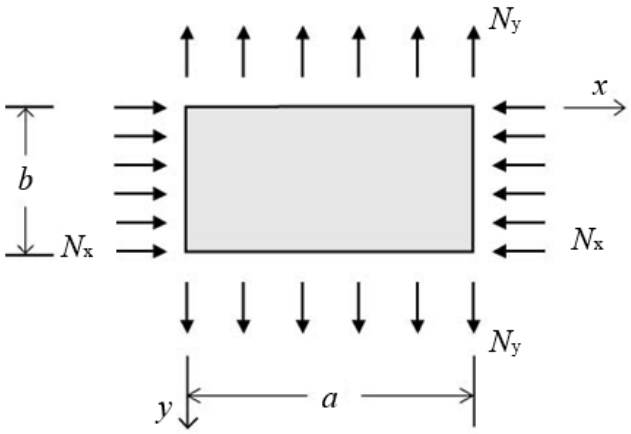

Figure 1. Rectangular composite panel under biaxial loading.

From Equation (21), the buckling load N_{cr} is a function of the number of half-waves m in the x direction and n in the y direction. $k > 0$ implies biaxial compression, then, negative values of k correspond to tensile N_y values. Furthermore, a tensile N_y ($k < 0$) tends to stabilize the plate and increase its buckling load [24]. In other words, the tensile load along the y direction is beneficial for improving the critical buckling load for a rectangular plate when the compressive load is applied in the x direction.

Usually, a simply supported boundary condition of uniaxial compression applied in the x direction does not include the in-plane translational restraint along the y direction for buckling analysis in the available literature. However, the ideal free boundary conditions for a simply supported plate never occur in practice, and therefore in-plane translational restraint exists. If the unloaded edges were to be subjected to elastic restraint against in-plane translation, then the induced equivalent load along the unloaded y direction would be compressive for the material with a positive Poisson's ratio, and would be tensile for the plate with a negative Poisson's ratio [17]. From Equation (21), it can be seen that if the plate has a negative in-plane Poisson's ratio and in-plane translational constraint is considered, the axial compression buckling load can be increased due to the induced tension force on the unloaded y direction.

According to Ref. [17], an elastic coefficient of support k was also employed to simulate constraint stiffness along the unloaded sides shown in Figure 2. α is defined as the in-plane translational restraint coefficient shown in Equation (22). Hence, the restraint coefficient α varies from 0 (free expansion condition) to 1 (full restrained condition).

$$\alpha = \frac{b/E_y}{t/k + b/E_y} \tag{22}$$

$$N_y = \alpha v_{yx} N_x \tag{23}$$

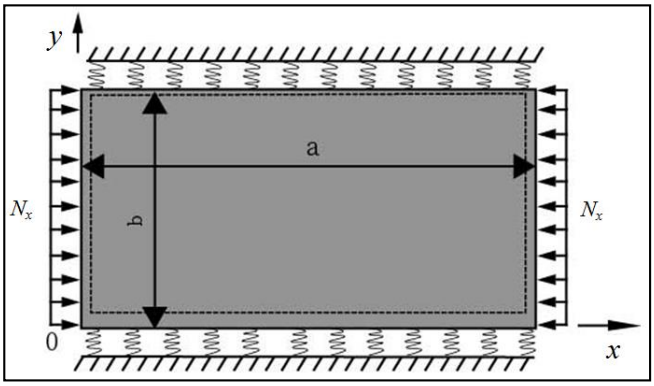

Figure 2. Uniaxial compressive plate elastically restrained along unloaded edges [17].

The critical buckling load of an orthotropic plate, with the induced equivalent load along the unloaded edges caused by the in-plane translational restraint, should be determined by:

$$N_x(m,n) = \frac{D_{11}(m\pi/a)^4 + 2(D_{12}+2D_{66})(m\pi/a)^2(n\pi/b)^2 + D_{22}(n\pi/b)^4}{(m\pi/a)^2 + \alpha\nu_{yx}(n\pi/b)^2} \quad (24)$$

4. Results and Discussion

4.1. Auxetic Design of Laminated Rectangular Plate with Membrane Lamination Parameters

In this section, feasible Poisson's ratios are discussed in the design space of the four membrane lamination parameters. All the layers are made from T300/5208 carbon–epoxy composites [9]; the material properties of the lamina are given in Table 1.

Table 1. Material properties of the lamina.

E_{11} (GPa)	E_{22} (GPa)	v_{12}	G_{12} (GPa)	ρ (kg/m^3)	t_{ply} (mm)
181	10.3	0.28	4.47	1580	0.1

The Poisson's ratio contours are plotted in Figure 3 on the following four planes in the design space of the four membrane lamination parameters (the Poisson's ratios are determined with an interval of 0.5 for lamination parameters):

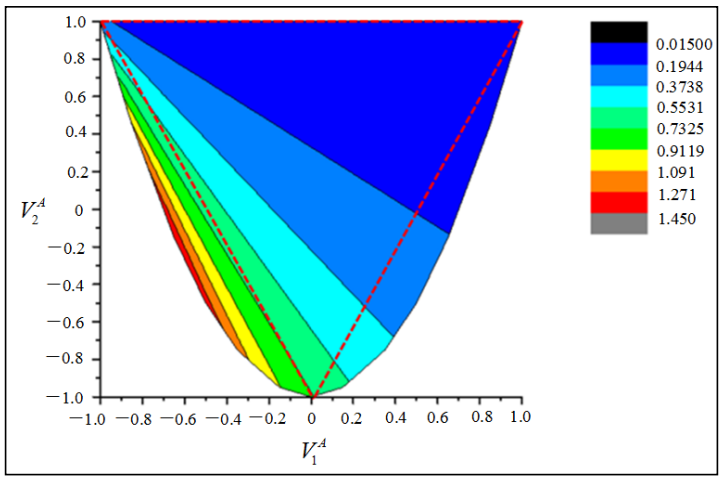

(**a**)

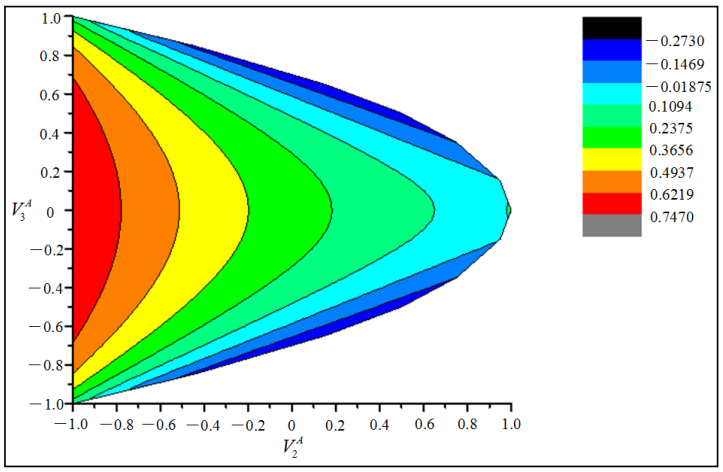

(**b**)

Figure 3. *Cont.*

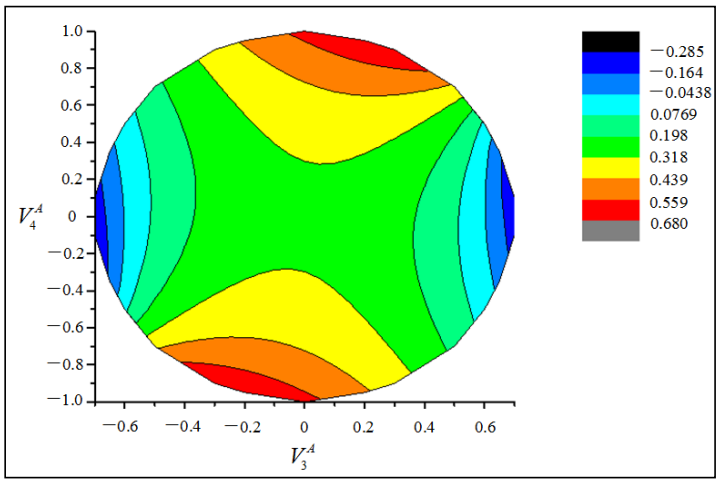

(**c**)

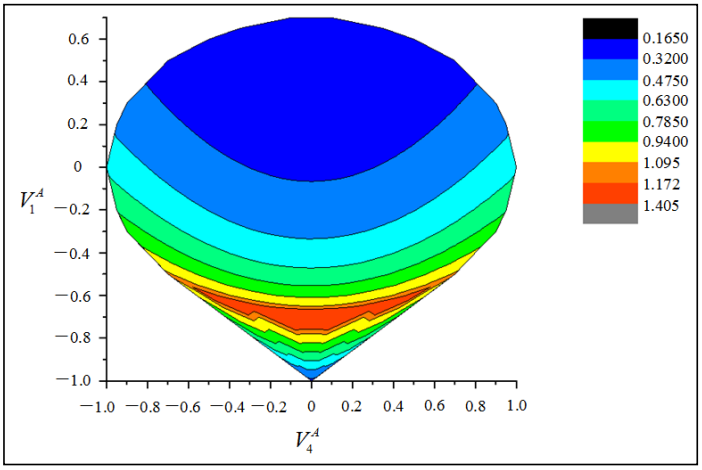

(**d**)

Figure 3. Contours of Poisson's ratio. (**a**) V_1^A, V_2^A plane for $V_3^A = V_4^A = 0$. (**b**) V_2^A, V_3^A plane for $V_1^A = V_4^A = 0$. (**c**) V_3^A, V_4^A plane for $V_1^A = V_2^A = 0$. (**d**) V_4^A, V_1^A plane for $V_2^A = V_3^A = 0$.

(a) V_1^A, V_2^A plane for $V_3^A = V_4^A = 0$.
(b) V_2^A, V_3^A plane for $V_1^A = V_4^A = 0$.
(c) V_3^A, V_4^A plane for $V_1^A = V_2^A = 0$.
(d) V_4^A, V_1^A plane for $V_2^A = V_3^A = 0$.

In each plane, the contours are shown in the feasible region of the membrane lamination parameters given by Equation (9). According to Figure 3a, the Poisson's ratios of the orthotropic laminate ($V_3^A = V_4^A = 0$) vary from 0.015 to 1.450, that is, the orthotropic laminate with $V_3^A = V_4^A = 0$ do not have the opportunity to obtain NPR no matter the ply angle or orientation change. According to Equation (6), for a laminate composed of 0°, 90°, 45°, and −45° fiber angles, the membrane lamination parameters can be formulated as follows:

$$V_1^A = \frac{n_0 - n_{90}}{n} \tag{25}$$

$$V_2^A = \frac{n_0 + n_{90} - n_{45} - n_{-45}}{n} \tag{26}$$

$$V_3^A = \frac{n_{45} - n_{-45}}{n} \tag{27}$$

where n denotes the number of total plies, and n_0, n_{90}, n_{45}, and n_{-45} denote the number of plies for 0°, 90°, 45°, and −45°, respectively. For the symmetric and balanced laminate composed of 0°, 90°, 45°, and −45° fiber angles, $V_3^A = V_4^A = 0$, the Poisson's ratio

of the laminate can be determined according to Figure 3a and Equations (25) and (26). Furthermore, the boundary of the feasible region for the orthtropic laminate composed of 0°, 90°, 45° and −45° fiber angles in the design space of V_1^A, V_2^A is also shown in Figure 3a by a red dashed line.

Comparing the Poisson's ratio contours on the four planes, it can be seen that the negative Poisson's ratio are more sensitive to V_3^A. V_3^A represents the unbalanced degree of a laminate. The NPR regions for the two-lamination parameter plane are also given in Figure 2. The minimum NPR is −0.360 for $[V_1^A, V_2^A, V_3^A, V_4^A] = [-0.35, 0.25, -0.6, 0.25]$ or $[-0.35, 0.25, 0.6, -0.25]$. The maximum NPR is 1.450 for $[V_1^A, V_2^A, V_3^A, V_4^A] = [-0.65, 0.15, 0, -0.05]$ or $[-0.65, 0.15, 0, 0.05]$. Compared with the other three NPR regions, the NPR points for V_2^A, V_3^A occupy the smallest proportion of whole V_2^A, V_3^A region, which reveals that the $V_2^A - V_3^A$ relationship takes the lead for NPR combinations of lamination parameters. NPR points for two-lamination parameter plane is shown in Figure 4.

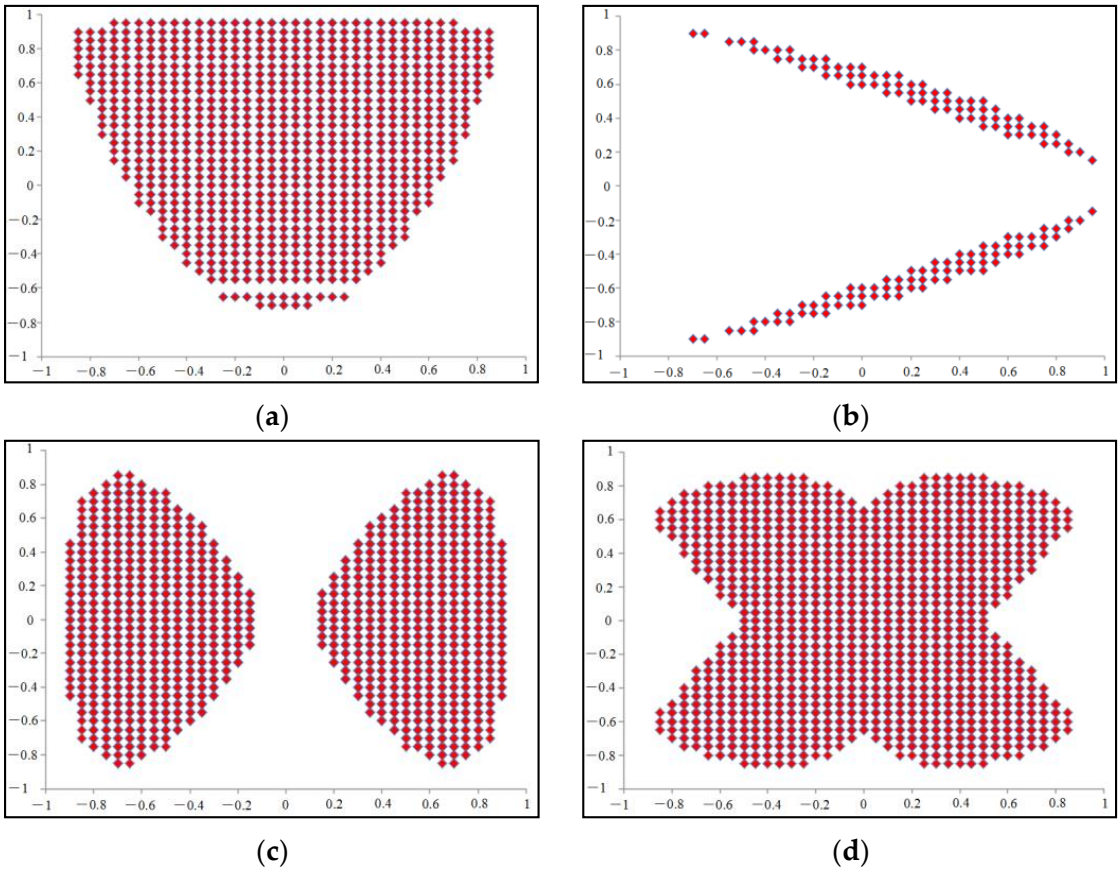

Figure 4. NPR points for two-lamination parameter plane. (**a**) NPR points for V_1^A, V_2^A. (**b**) NPR points for V_2^A, V_3^A. (**c**) NPR points for V_3^A, V_4^A. (**d**) NPR points for V_4^A, V_1^A.

4.2. Buckling Load Intensity for Various Poisson's Ratio Layup

The buckling load intensity with bending lamination parameters for various Poisson's ratio layups were investigated. The geometry of the chosen plate is 100 mm × 100 mm and the thickness is 2 mm.

Firstly, the minimum NPR of −0.360 with $[V_1^A, V_2^A, V_3^A, V_4^A] = [-0.35, 0.25, -0.6, 0.25]$ was selected for the buckling load investigation. According to the feasible region of Equation (9), different combinations of bending lamination parameters can be obtained with $[V_1^A, V_2^A, V_3^A, V_4^A] = [-0.35, 0.25, -0.6, 0.25]$. Note that the buckling load Equation (24) assumes that the bending–twisting coupling terms D_{16} and D_{26} are negligible compared with the remaining terms D_{11}, D_{12}, D_{22}, and D_{66}. Therefore, it is better to calculate the buckling load for the laminate configuration with $V_3^D = V_4^D = 0$. However, the lamination parameter combination of $[V_1^A, V_2^A, V_3^A, V_4^A, V_3^D, V_4^D] = [-0.35, 0.25, -0.6, 0.25, 0, 0]$

does not satisfy the feasible region of lamination parameters. Thus, a combination of $V_3^D = 0.05$, $V_4^D = 0$ to ensure the orthotropic condition to the highest extent is used to illustrate the V_1^D, V_2^D plane for the buckling load contours.

From the buckling load contours of Figure 5, two different buckling models may exist in the whole region of V_1^D, V_2^D. Four sets as follows are chosen to examine the effect of lamination parameters on the buckling modes:

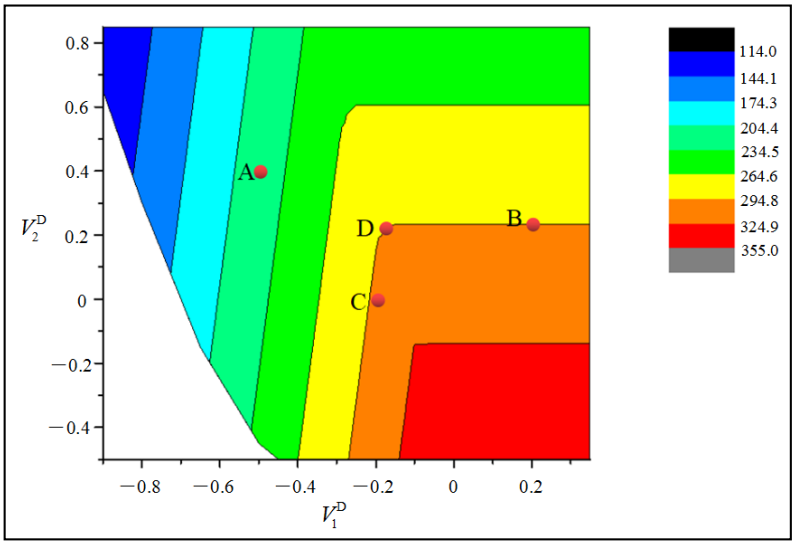

Figure 5. Plane for $[V_1^A, V_2^A, V_3^A, V_4^A, V_3^D, V_4^D] = [-0.35, 0.25, -0.6, 0.25, 0, 0]$.

Point A: $[V_1^A, V_2^A, V_3^A, V_4^A, V_1^D, V_2^D, V_3^D, V_4^D] = [-0.35\ 0.25\ -0.6\ 0.25\ -0.5\ 0.4\ -0.05\ 0]$.
Point B: $[V_1^A, V_2^A, V_3^A, V_4^A, V_1^D, V_2^D, V_3^D, V_4^D] = [-0.35\ 0.25\ -0.6\ 0.25\ 0.2\ 0.2\ -0.05\ 0]$.
Point C: $[V_1^A, V_2^A, V_3^A, V_4^A, V_1^D, V_2^D, V_3^D, V_4^D] = [-0.35\ 0.25\ -0.6\ 0.25\ -0.2\ 0\ -0.05\ 0]$.
Point D: $[V_1^A, V_2^A, V_3^A, V_4^A, V_1^D, V_2^D, V_3^D, V_4^D] = [-0.35\ 0.25\ -0.6\ 0.25\ -0.2\ 0.2\ -0.05\ 0]$.

The buckling modes of point A and point C are consistent; there are two half wavelengths in the x direction (m = 2) and one in the y direction (n = 1), while there is one half wavelength in x direction (m = 1) and one in y direction (n = 1) for point B. Point D is the dividing point of the two buckling modes. When m = 2, n = 1 or m = 1, n = 1, the buckling load is the same. The buckling mode is not only related to the stiffness, but also to the aspect ratio of the plate. The buckling load contour lines for 200 mm × 100 mm and 300 mm × 100 mm plates are given in Figures 6 and 7, respectively.

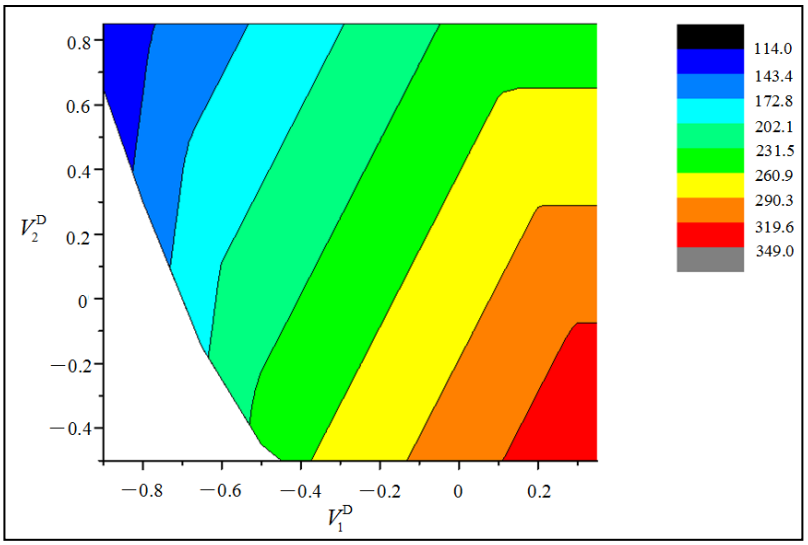

Figure 6. Plane for 200 × 100 mm plate.

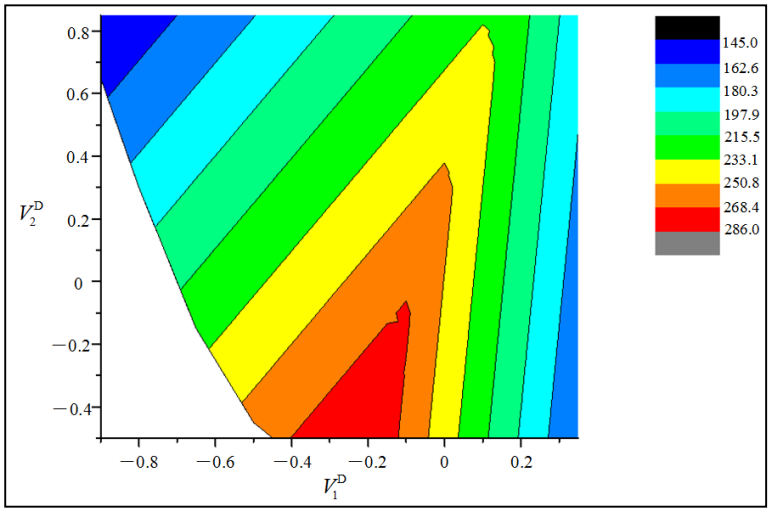

Figure 7. Plane for 300 × 100 mm plate.

Secondly, the lamination parameters of $[V_1^A, V_2^A, V_3^A, V_4^A] = [0.4, -0.05, -0.6, -0.1]$ with a PR of 0, and $[V_1^A, V_2^A, V_3^A, V_4^A] = [0, 0, 0, 0]$ with a PR of 0.296, are both studied for buckling load with various bending lamination parameters combinations. It can be seen from the contours that the buckling load is almost only related to V_2^D. The buckling load decreases with an increase in V_2^D. From Figures 5 and 8, the possible maximum buckling load decreases with an increase in Poisson's ratio.

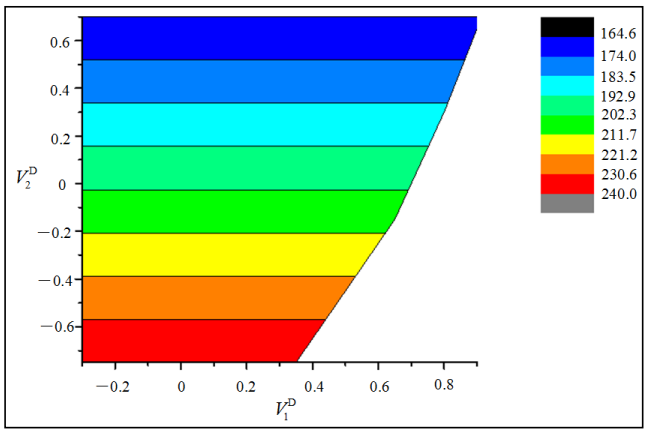

(**a**)

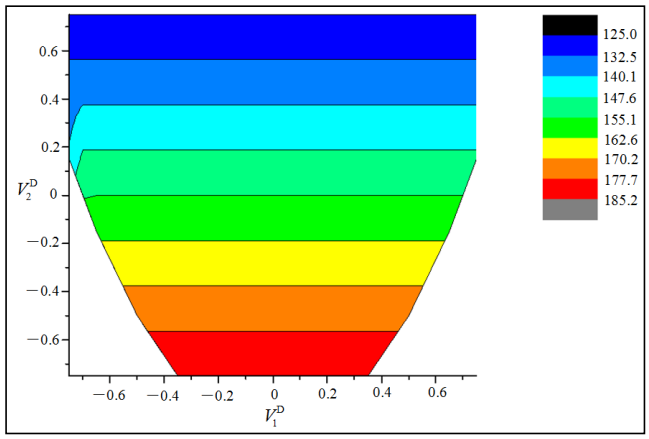

(**b**)

Figure 8. Plane for various $[V_1^A, V_2^A, V_3^A, V_4^A, V_1^D, V_2^D]$. (**a**) V_1^D, V_2^D plane for $[0.4, -0.05, -0.6, -0.1, 0, 0]$. (**b**) V_1^D, V_2^D plane for $[0, 0, 0, 0, 0, 0]$.

The influence of Poisson's ratio and the in-plane translational restraint coefficient on the buckling load of quasi isotropic laminates ($[V_1^A, V_2^A, V_3^A, V_4^A] = [0,0,0,0]$) was studied. α is the in-plane translational restraint coefficient, which represents the degree of translational limitation. Figure 9 reveals the variation of the buckling loads of the rectangular plate with the Poisson's ratio for different in-plane translational restraint coefficients. The buckling load remains unchanged when the restraint coefficient α equals zero and, when the Poisson's ratio is zero, the buckling load is the same for various restraint coefficients. If the in-plane translational restraint exists ($\alpha > 0$), the buckling load gradually decreases as the Poisson's ratio increases. These results imply that the buckling load is a decreasing function of the laminate's Poisson's ratio, and hence the buckling performance of a rectangular plate under uniaxial compression can be enhanced by replacing the traditional layup that has a positive Poisson's ratio with an auxetic design.

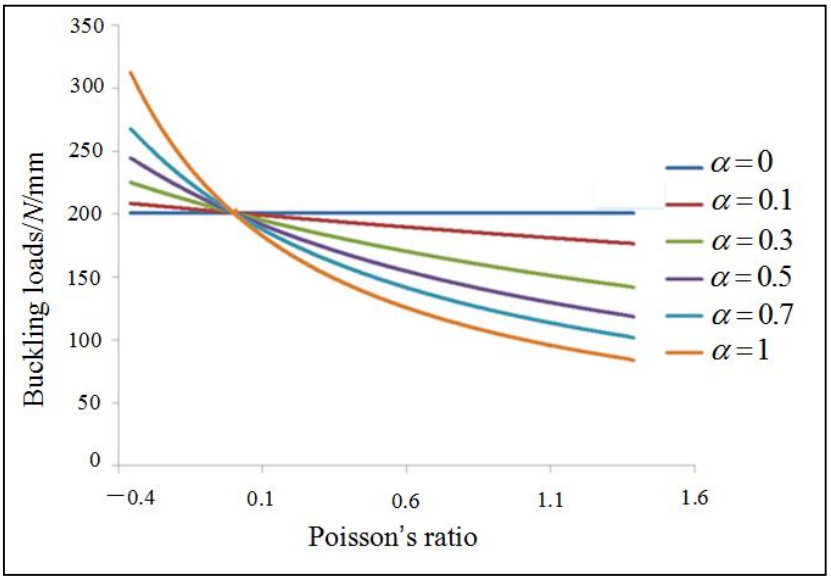

Figure 9. Buckling loads with Poisson's ratio for various in-plane translational restraint coefficients.

4.3. Inverse Problem of Laminate Configuration

The inverse problem of deciding the laminate configuration to target the lamination parameters for three sets was investigated:

(a) $[V_1^A, V_2^A, V_3^A, V_4^A] = [-0.45, 0.35, -0.55, 0.3]$ with PR of -0.356.
(b) $[V_1^A, V_2^A, V_3^A, V_4^A] = [0,0,0,0]$ with PR of 0.296.
(c) $[V_1^A, V_2^A, V_3^A, V_4^A] = [-0.55, -0.35, 0.05, -0.3]$ with PR of 1.389.

The relationship between the lamination parameters and the stacking sequence is not always unique; there is no closed-form solution to convert a point in the lamination parameters' space into a stacking sequence. Further still, when prescribing the number of layers in the laminate, certain points in the lamination parameters' space do not have a corresponding layup, and the closest alternative must be found. In previous work, the conversion process was formulated as an optimization problem. The objective function that was used for this optimization was the least rectangular distance of the lamination parameters to the desired optimum point:

$$\begin{aligned} &\min f(\theta) = \sum_{i=1}^{4} \left[\left(V_i^A - V_{iopt}^A \right)^2 + \left(V_i^D - V_{iopt}^D \right)^2 \right] \\ &s.t. \quad \theta \in \{\text{from} -90^o \text{ to } 90^o \text{ with an interval of 5 degrees}\} \end{aligned} \tag{28}$$

where *opt* denotes the given optimum lamination parameters.

Due to its ability to deal with the continuous global optimization problem with a non-linear objective function, particle swarm optimization (PSO) is an evolutionary global

algorithm that has become more and more popular. PSO was first proposed by Kennedy and Eberhart [26,27]. It is observed that a swarm of birds or insects searches for food in a very typical manner. If one member of the swarm finds a desirable path to go, the rest of the particles will follow quickly. Each particle searches for the best in its locality with learning from its own experience. Additionally, each member learns from the others, typically from the best performer among them. PSO has been successfully applied to some engineering and structural problems.

The basic steps in the PSO algorithm are as follows:

Step 1 Initialize the swarm with random position values and random initial velocities.

Step 2 Determine the velocity vector for each particle in the swarm using the knowledge of the best position obtained by each particle and the swarm as a whole, and also the previous position of each particle in the swarm.

Step 3 Modify the current position of each particle using the velocity vector and the previous position of each particle.

Step 4 Repeat from step 2 until the stop criterion is achieved.

The velocity vector of each particle is calculated as follows:

$$v_k^i = wv_{k-1}^i + c_1 r_1 (p^i - x_{k-1}^i) + c_2 r_2 (p_{k-1}^g - x_{k-1}^i) \tag{29}$$

where the superscript i denotes the particle and the subscript k denotes the iteration number; v denotes the velocity and x denotes the position; r_1 and r_2 are uniformly distributed random numbers in the interval [0, 1]; c_1 and c_2 are the acceleration constants; w is the inertia weight; p^i is the best position attained by the particle i in the swarm so far; and p_{k-1}^g is the global best position attained by the swarm at iteration $k-1$.

The position of each particle at iteration k is calculated using the formula:

$$x_k^i = x_{k-1}^i + v_k^i \tag{30}$$

The laminate configurations for various lamination parameters were obtained, as shown in Table 2. For example, with a thickness of 2 mm and lamination parameters of $[V_1^A, V_2^A, V_3^A, V_4^A, V_1^D, V_2^D, V_3^D, V_4^D] = [-0.45, 0.35, -0.55, 0.3, 0, 0, 0, 0]$, the corresponding stacking sequence of laminate can be obtained, $[-15/40/-85/-75/60/0/75/-50/-15/35]_s$; the objective of the least rectangular distance of the lamination parameters to the desired optimum point is 0.058 in Equation (28).

Table 2. Laminate configurations for lamination parameters.

Target Lamination Parameters	Real Lamination Parameters	Laminate Configuration	Objective
[−0.45, 0.35, −0.55, 0.3, 0, 0, 0, 0]	[−0.43, 0.29, −0.35, 0.36, −0.01, −0.03, −0.09, 0.003]	$[-15/40/-85/-75/60/0/-75/-50/-15/35]_s$	0.058
[0, 0, 0, 0, 0, 0, 0, 0]	[0.0019, −0.0075, 0.0086, −0.017, −0.020, −0.0006, −0.0084, 0.0028]	$[65/65/30/5/-85/-85/-20/-85/-85/80]_s$	0.0009
[−0.55, −0.35, 0.05, −0.3, 0, 0, 0, 0]	[−0.34, −0.26, 0.062, −0.27, −0.048, −0.043, −0.012, −0.031]	$[-85/75/-35/50/30/-10/-70/-10/-30/0]_s$	0.06

5. Conclusions

Laminated structures can obtain an NPR effect by the proper orientation or a stacking sequence of laminate layers. The aim of this paper was to study the buckling load enhancement of an auxetic laminated plate under uniaxial compression considering in-plane translational restraint. Four membrane lamination parameters were employed to study the feasible regions for the Poisson's ratios. The results show that it is impossible for an orthotropic plate to have a negative Poisson's ratio, and negative Poisson's ratios are more sensitive to V_3^A, which denotes the unbalanced degree. Furthermore, the influence of the Poisson's ratio and in-plane translational restraint coefficient on the buckling load has been studied, which reveals that the buckling performance of a rectangular plate under uniaxial compression can be enhanced with an auxetic design. Finally, PSO is efficient for the inverse problem of deciding the laminate configuration to target the lamination parameters.

Author Contributions: Conceptualization, K.W. and F.W.; methodology, L.L.; software, P.C. and L.H.; validation, P.J., K.W. and L.L.; formal analysis, F.W.; resources, P.J.; data curation, L.L.; writing—original draft preparation, K.W.; writing—review and editing, F.W., P.J. and L.L.; project administration, K.W. All authors have read and agreed to the published version of the manuscript.

Funding: This research was funded by the National Natural Science Foundation of China (NSFC) under grant number 12172141.

Institutional Review Board Statement: The study did not require ethical approval.

Informed Consent Statement: The study did not involve humans.

Data Availability Statement: The relevant data is already included in the article, and no additional data is required.

Conflicts of Interest: The authors declare no conflict of interest.

References

1. Surjadi, J.U.; Gao, L.; Du, H.; Li, X.; Xiong, X.; Fang, N.X.; Lu, Y. Mechanical Metamaterials and Their Engineering Applications. *Adv. Eng. Mater.* **2019**, *21*, 1800864. [CrossRef]
2. Ren, X.; Das, R.; Tran, P.; Ngo, T.D.; Xie, Y.M. Auxetic metamaterials and structures: A review. *Smart Mater. Struct.* **2018**, *27*, 023001. [CrossRef]
3. Jiang, J.-W.; Kim, S.Y.; Park, H.S. Auxetic nanomaterials: Recent progress and future development. *Appl. Phys. Rev.* **2016**, *3*, 041101. [CrossRef]
4. Saxena, K.K.; Das, R.; Calius, E.P. Three Decades of Auxetics Research—Materials with Negative Poisson's Ratio: A Review. *Adv. Eng. Mater.* **2016**, *18*, 1847–1870. [CrossRef]
5. Lakes, R.S. Negative-Poisson's-Ratio Materials: Auxetic Solids. *Annu. Rev. Mater. Res.* **2017**, *47*, 63–81. [CrossRef]
6. Lakes, R. Foam Structures with a Negative Poisson's Ratio. *Science* **1987**, *235*, 1038–1040. [CrossRef]
7. Hu, C.; Dong, J.; Luo, J.; Qin, Q.-H.; Sun, G. 3D printing of chiral carbon fiber reinforced polylactic acid composites with negative Poisson's ratios. *Compos. Part B Eng.* **2020**, *201*, 108400. [CrossRef]
8. Wang, Z.; Hu, H. Auxetic materials and their potential applications in textiles. *Text. Res. J.* **2014**, *84*, 1600–1611. [CrossRef]
9. Shokrieh, M.M.; Assadi, A. Determination of maximum negative Poisson's ratio for laminated fiber composites. *Phys. Status Solidi* **2011**, *248*, 1237–1241. [CrossRef]
10. Herakovich, C.T. Composite Laminates with Negative Through-the-Thickness Poisson's Ratios. *J. Compos. Mater.* **1984**, *18*, 447–455. [CrossRef]
11. Azoti, W.; Koutsawa, Y.; Bonfoh, N.; Lipinski, P.; Belouettar, S. Analytical modeling of multilayered dynamic sandwich composites embedded with auxetic layers. *Eng. Struct.* **2013**, *57*, 248–253. [CrossRef]
12. Chen, X.; Feng, Z. Dynamic behaviour of a thin laminated plate embedded with auxetic layers subject to in-plane excitation. *Mech. Res. Commun.* **2017**, *85*, 45–52. [CrossRef]
13. Alderson, K.L.; Coenen, V.L. The low velocity impact response of auxetic carbon fibre laminates. *Phys. Status Solidi* **2008**, *245*, 489–496. [CrossRef]
14. Miki, M.; Murotsu, Y. The Peculiar Behavior of the Poisson's Ratio of Laminated Fibrous Composites. *JSME Int. J.* **1989**, *32*, 67–72. [CrossRef]
15. Kiarasi, F.; Babaei, M.; Asemi, K.; Dimitri, R.; Tornabene, F. Three-Dimensional Buckling Analysis of Functionally Graded Saturated Porous Rectangular Plates under Combined Loading Conditions. *Appl. Sci.* **2021**, *11*, 10434. [CrossRef]
16. Kiarasi, F.; Babaei, M.; Dimitri, R.; Tornabene, F. Hygrothermal modeling of the buckling behavior of sandwich plates with nanocomposite face sheets resting on a Pasternak foundation. *Contin. Mech. Thermodyn.* **2021**, *33*, 911–932. [CrossRef]
17. Zhang, Y.; Li, X.; Liu, S. Enhancing buckling capacity of a rectangular plate under uniaxial compression by utilizing an auxetic material. *Chin. J. Aeronaut.* **2016**, *29*, 945–951. [CrossRef]
18. Shen, H.-S.; Xiang, Y. Effect of negative Poisson's ratio on the postbuckling behavior of pressure-loaded FG-GRMMC laminated cylindrical shells. *Eng. Struct.* **2021**, *243*, 112458. [CrossRef]
19. Shen, H.-S.; Xiang, Y.; Reddy, J. Effect of negative Poisson's ratio on the post-buckling behavior of FG-GRMMC laminated plates in thermal environments. *Compos. Struct.* **2020**, *253*, 112731. [CrossRef]
20. Kassapoglou, C. *Design and Analysis of Composite Structures: With Applications to Aerospace Structures*; John Wiley & Sons Ltd.: Hoboken, NJ, USA, 2013.
21. Kameyama, M.; Arai, M. Optimal design of symmetrically laminated plates for damping characteristics using lamination parameters. *Compos. Struct.* **2015**, *132*, 885–897. [CrossRef]
22. Diaconu, C.G.; Sato, M.; Sekine, H. Buckling characteristics and layup optimization of long laminated composite cylindrical shells subjected to combined loads using lamination parameters. *Compos. Struct.* **2002**, *58*, 423–433. [CrossRef]
23. Diaconu, C.G.; Sekine, H. Layup Optimization for Buckling of Laminated Composite Shells with Restricted Layer Angles. *AIAA J.* **2004**, *42*, 2153–2163. [CrossRef]

24. Megson, T. *Aircraft Structures for Engineering Students*, 6th ed.; Springer: Berlin/Heidelberg, Germany, 2017.
25. Whitney, J. *Structural Analysis of Laminated Anisotropic Plates*; Technomic Publishing: Lancaster, PA, USA, 1987.
26. Kennedy, J.; Eberhart, R. Particle Swarm Optimization. In Proceedings of the IEEE International Conference on Neural Networks, Perth, Australia, 27 November–1 December 1995; Volume 4, pp. 1942–1948. [CrossRef]
27. Eberhart, R.; Kennedy, J. A new optimizer using particle swarm theory. In Proceedings of the Sixth International Symposium on Micro Machine and Human Science (MHS'95), Nagoya, Japan, 4–6 October 1995; pp. 39–43. [CrossRef]